# Quasicontinuum study of the shear behavior of defective tilt grain boundaries in Cu

V. Péron-Lührs[a], F. Sansoz[b,*], L. Noels[a,*]

[a] *University of Liege, Department of Aerospace and Mechanical Engineering - Computational & Multiscale Mechanics of Materials, Chemin des Chevreuils 1, B4000 Liège Belgium*
[b] *Mechanical engineering and materials science programs, School of Engineering, The University of Vermont, Burlington, VT 05405, USA.*

**Abstract**

Atomistic simulations using the quasicontinuum method are used to study the role of vacancy defects and angström-scale voids on the mechanical behavior of five tilt bicrystals containing grain boundaries (GBs) that have been predicted to exhibit characteristic deformation processes of nanocrystalline and nanotwinned metals : GB-mediated dislocation emission, interface sliding, and shear-coupled GB migration. We demonstrate that such nanoscale defects have a profound impact on interfacial shear strength and underlying deformation mechanisms in copper GBs due to void-induced local stresses. In asymmetric high and low angle GBs, we find that voids become preferential sites for dislocation nucleation when the void size exceeds 4 Å. In symmetric $\Sigma9(221)$ GBs prone to sliding, voids are shown to shield the local shear stress, which considerably reduces the extent of atom shuffling at the interface. In symmetric $\Sigma5(210)$ and $\Sigma27(115)$ GBs, we find that the effect of voids on shear-coupled GB migration depends on the GB tilt direction considered, as well as on the size and number of voids. Remarkably, large voids can completely abate the GB migration process in $\Sigma27(115)$ GBs. For all GB types, the interfacial shear strength is shown to decrease linearly as the volume fraction of voids at the interface increases ; however, this study also suggests that this decrease is much more pronounced in GBs deforming by sliding than by dislocation nucleation or migration, owing to larger void-induced stresses.

*Keywords:* Grain boundary defects, Grain boundary structure, Yield phenomena, Copper,

## 1. Introduction

Local point defects such as nanovoids and vacancies present in grain boundaries (GBs) play an important role at the macroscopic level for the yield, plasticity, and fracture behavior of polycrystalline and nanocrystalline metals. In pure tension, growth and coalescence of nanovoids smaller than a few nm in diameter can participate collectively in shear band formation and localized plastic deformation processes that result in significant material softening in metals [1–4]. It is also now well-accepted that the mechanical behavior of GB networks governs the plastic deformation of nanocrystalline and nanotwinned metals due to GB-induced mechanisms, such as GB migration [5–10], dislocation nucleation [11–14], and interface sliding [10, 11, 14–17]. However, recent investigations focusing on the atomic-scale structure of GBs by nanodiffraction [18, 19] have revealed experimentally that columnar grains in nanotwinned Cu have GBs with curves and defects that have not been observed in previous studies. Yet these defected GBs strongly differ from the models obtained by classical Voronoï construction that have been traditionally considered in atomistic simulation studies [20], whereas their impact on the constitutive behavior of metals is not fully understood at present.

Computer simulations can provide further quantitative insights into the role of voids on the mechanical behavior and underlying deformation mechanisms at GBs. The intrinsic mechanisms associated with the elastic-plastic deformation of nanosized voids, or nanovoids, in metals have been investigated previously by classical molecular dynamics (MD) simulations and mixed atomistic-finite element simulations [21–24]. Past MD studies have focused on

∗. Corresponding authors, Phone : +32 4 366 48 26 (L.Noels) +1 802 656 3837 (F. Sansoz), Fax : +32 4 366 95 05 (L.Noels) +1 802 656 1929 (F. Sansoz)

*Email addresses:* Vincent.Peron-Luhrs@ulg.ac.be (V. Péron-Lührs), Frederic.Sansoz@uvm.edu (F. Sansoz), L.Noels@ulg.ac.be (L. Noels)

the dislocation dynamics in growth and coalescence of voids in single crystals [25]. Moreover, a recent MD study [26] has proposed a new methodology considering the atomistic density inside GBs by adding interstitial atoms or vacancies, and revealed multiple GB phases with different atomic structures. However, this latter study did not specifically address the impact of vacancies on the deformation modes and mechanical response of GBs. Also, atomistic simulations using the quasicontinuum (QC) method [27, 28] have been performed to study the shearing of perfect crystalline interfaces with no defects [27, 29–31], as well as the effect of nanovoids in single crystals, i.e. without considering GBs [32]. However, although first-principles calculations have shown that nanovoids locally induce significant stresses in pure diamond GBs [33], their effect on the GB strength and deformation mechanisms in metals has not been investigated so far.

To close this gap, the present study employs atomistic simulations using the QC method to examine the shear behavior of defective tilt GBs. The QC approach is a well-established method in the study of GB deformation in bicrystals as shown by past works [29, 30]. In particular, the QC method was used in the very first study reporting the important role of E structural units in mediating GB sliding and GB-mediated dislocation nucleation, confirmed later by more complex MD simulations at finite temperature [34]. It is worth noting that these structural units represent a sub-category of free volume in GBs, similar to the angström-scale voids discussed below, justifying the use of the QC method. Furthermore, the main purpose of the quasi-2D models used in this work is to simulate intrinsic deformation processes in tilt GBs, rather than to focus on the structure of dislocations emanating from the GBs which would require a 3D analysis; thereby allowing us to save significant computational resources while remaining within the domain of validity of 2D GB models used [35, 36].

In this paper, three special symmetric tilt structures with either a $<1\bar{1}0>$ or $<100>$ tilt direction in addition to two general asymmetric $<1\bar{1}0>$ GBs with either a low or high miso-

3

rientation angle, respectively referred to as LAB and HAB in the following, are investigated. Here, we show that GB vacancy defects result in a significant decrease in the maximum shear resistance for each GB type in Cu as the void volume fraction increases with the number and size of voids, and that nanovoid-induced stresses can dramatically alter the deformation mechanisms of GBs. In light of these results, a theoretical model taking into account the degree of alteration based on the void volume fraction is proposed.

The paper is organized as follows. Section 2 presents the details of the computational procedure used to simulate perfect and defective GBs undergoing simple shear loads. Section 3 is devoted to results showing that the incipient plasticity and associated deformation mechanisms taking place in these GBs depend on the size and number of voids. In Section 4, the effect of nanovoids on the deformation mechanisms of GBs is discussed, and a model predicting the shear behavior of defective GBs based on the void volume fraction is presented.

## 2. Computational methodology

Shearing of GBs was modeled using QC simulations of tilt bicrystals strained under simple shear following the methodology described in previous studies [29, 30]. QC models of 2D tilt GBs were created by projection of the 3D crystallography orientations along the $<1\bar{1}0>$ or $<100>$ directions. Special boundaries were represented by coincident site lattice (CSL) GBs with low $\Sigma$ values corresponding to the reciprocal density of coincident atoms [37, 38]. We considered a $\Sigma 9(221)$ GB, which has previously been predicted to simulate GB sliding by atomic shuffling [30], and a $\Sigma 27(115)$ prone to shear-coupled GB migration with a $<1\bar{1}0>$ tilt axis, as well as a $\Sigma 5(210)$ GB (also prone to migration) with a $<100>$ tilt axis. For general GBs, LABs have been considered as GBs with misorientation angles lower than 10 degrees [39], or between 9 and 14 degrees [40]. In this study, the LAB and HAB chosen were $[0\ 0\ \overline{10}]/[1\ 1\ 10]$ and $[\overline{1}\overline{1}0]/[\overline{3}\ \overline{3}\ 10]$ interfaces with a misorientation angle equal to $0.8°$ and $111.53°$, respectively.

The grains were treated as a continuum medium by the finite element method, while a full atomic resolution was kept around the crystalline interfaces within a distance equal to 6 times the potential cutoff as shown in Figure 1. Face-centered cubic (fcc) Cu atoms were modeled using the embedded-atom-method (EAM) based on the potential defined by Foiles et al. [41, 42] with a cutoff distance of 4.950 Å (at 0 K). A relaxation under zero load with all atoms kept free of constraints, except for those at the bottom of the lower grain, was performed prior to deformation. The total energy was minimized by a conjugate gradient method until the addition of out-of-balance forces over the entire system was below $10^{-3}$ eV/Å$^3$. For all GBs, different initial grain shifts were tested and only GB configurations with the lowest energy configurations after relaxation are considered in this work. A gap of 3 Å between the upper and lower grains, see Figures 1(b) and (c), was initially used to improve the convergence toward these low-energy configurations. Circular voids were created in the GBs by removing GB atoms. Each void consisted of 2 to 22 vacancies, and was shaped as a column passing through the model (due to the 2D constraint imposed by the QC model). The number of voids at the interface was varied from 2 to 16 on a GB length of 600 Å, while the void size (diameter) was varied from 4 to 10 Å. An example of simulated $\Sigma 9(221)$ GB containing 4 voids is shown before relaxation in Figure 1(c). The shape of the voids were found to change during the relaxation process, but the larger the diameter, the more circular the shape after relaxation. Also, void position was uniformly distributed at the interface and did not follow the GB periodicity. Although voids were sensibly different from one another for the same GB simulation, this approach allowed us to compare all GBs with similar defect patterns.

After the structure was relaxed, shearing was imposed by displacing the topmost row of nodes in the finite element mesh by increments of 0.1 Å, and by minimizing the energy between each loading step. The effective shear stress in the bicrystal was computed by adding the residual forces at the top of the upper grain and dividing this sum by the total cross-

sectional area. Also, previous MD studies have shown that free surfaces can be responsible for spurious effects; for example surface dislocation nucleation in MD studies when dealing with shear loadings [43]. Therefore, a domain including only 80% of the model and excluding all atoms near free surfaces on the left and right hand sides of the GB, was considered in the force and energy calculations in the present study. Moreover and to this end, the mesh aspect ratio was kept close to 6 (i.e. $\Delta_X \times \Delta_Y = 600$ Å$\times$ 100 Å). The shear strain was computed following [30]. The centrosymmetry parameter [44] was used to visualize atoms at interfaces and near defects, which will appear in darker color in the following, see Figure 1(c).

## 3. Results

### 3.1. Dependence of shear stress on the number and size of voids

Shown in Figure 2 are the simulated stress-strain curves for the 5 types of GBs studied in the absence of voids. Each bicrystal is found to deform elastically until the simulation cell reaches the stress $\sigma_{max_0}$, which represents the critical shear stress for the inception of plastic deformation or limit of elasticity. This figure shows that LAB and HAB interfaces attain higher stresses than the other GBs and yield at $\sigma_{max_0} = 4.08$ and 3.45 GPa, respectively. Table 1 shows that in decreasing order, $\sigma_{max_0} = 3.07, 1.35$, and 0.60 GPa in the $\Sigma 27(115)$, $\Sigma 9(221)$, and $\Sigma 5(210)$ GBs, respectively. These results agree with past studies that have shown that GB networks consisting mostly of HABs possess a smaller yield stress than those with special interfaces or LABs [31], and that shear-coupled GB migrations can occur at smaller stress than GB-mediated dislocation emissions [30].

Furthermore when considering nanovoids at the interfaces, we find in Figure 3 that the maximum shear stress decreases gradually for each GB structure as the number and size of voids increase. This result suggests that the maximum shear strength is dependent on the void volume fraction in the GB, as discussed in detail below.

6

## 3.2. Deformation mechanisms

GB networks govern the plastic deformation of nanocrystalline and nanotwinned metals due to several GB-induced mechanisms [45]. In this study, particular focus is paid to the processes of GB-mediated dislocation emission in HABs and LABs, GB sliding in $\Sigma 9(221)$ GBs, and GB migration in $\Sigma 5(210)$ and $\Sigma 27(115)$ GBs. Table 2 summarizes all the deformation mechanisms observed in these GBs as a function of the number and size of voids.

### 3.2.1. GB-mediated dislocation nucleation

Figure 4 shows that yielding in both HAB and LAB interfaces with no voids is controlled by the nucleation and propagation of partial dislocations from intrinsic GB sites (referred to as ED for emission from periodic defects), which are either mismatch interface dislocations in LAB or zones with large free volumes in HAB. For defective LAB and HAB, see Table 2, the same deformation mechanism is observed for void sizes up to 4 Å, for which yielding is activated from the ED process. When void sizes are equal to 10 Å, plasticity at the yield point corresponds to the emission of dislocation from voids, or EV, for both GB types. Therefore, we conclude that dislocations are emitted from voids when they are large enough, similar to the underlying mechanical process experimentally assumed in [2]. On the contrary, differences are found for HAB and LAB interfaces for intermediate void sizes. In the HAB interface both GB sites with large free volume and nanovoids (ED+EV) are found to emit dislocations at the same time when $\sigma_{max_0}$ is reached, regardless of the number of voids. In the LAB case however, the EV process gains the upper hand on the ED one sooner than in the HAB case.

### 3.2.2. GB sliding by atom shuffling

The representative GB of the shuffling process is the $\Sigma 9(221)$ GB, a mechanism already well documented in the literature [29, 30]. In Figure 5(a), for which no voids are involved, the entire interface is driven at the yield point by a periodic displacement of GB atoms to fill

free volumes called here homogeneous shuffling (HS). Shuffling becomes partial (PS) when voids are introduced as shown in Figure 5(b). In the latter case, voids act as strong pinning points against shuffling. Also, when voids become large, e.g. a $\Sigma9(221)$ GB with 8 voids of size 10 Å, Table 2 shows that the incipient plasticity is activated from voids by partial dislocation emission (EV).

### 3.2.3. Shear-coupled GB migration

Figures 6(a) and (b) prove that the yielding of the $\Sigma5(210)$ GB with no voids is associated with shear-coupled GB migration. Here this mechanism is referred to as homogeneous and total (HT) migration, that is, occurring all along the GB length and at once, respectively. Turning to the deformation of this GB in the presence of voids, Figures 6(c), 6(d) and 6(e) reveal several changes that have never been reported in the literature. For a void size equal to 8 Å, two different mechanisms are observed depending on the number of voids. In Figure 6(c), homogeneous and partial GB migration (HP) is identified in models with 4 voids : one segment of the GB located between 2 voids migrates homogeneously before other segments. In models with 8 voids (size 8 Å and above), Figures 6(d) and (e), inhomogeneous and partial migration (IP) is found and the ligament of material between two voids migrates inhomogeneously. Therefore, there exists a critical distance $D_V$ between voids for which the migration mechanism changes. This distance appears to be related to the size of voids.

The $\Sigma27(115)$ GB shown in Figure 7(a), is also representative of the GB migration mechanism. For this GB type, when the void size changes from 4 Å to 6 Å, the process moves from HT to HP or to IP, for 4 or 8 voids, respectively. Therefore, the same mechanism evolution is observed but with the exception that these changes occur for smaller voids (6 Å instead of 8 Å). Furthermore, we find a peculiar behavior for which the incipient plasticity is accompanied by dislocation emission from voids (EV), Figure 7(b). This phenomenon was not observed in the $\Sigma5(210)$ GB because the migration front rises in the upper grain without any dislocation emission, leaving reshaped voids behind with perfect fcc crystal

lattice around them, as shown in Figures 6(g) and 6(f).

## 4. Discussion

### 4.1. Influence of nanovoids on deformation mechanisms

The results of this study show that the presence of angström-scale voids in crystalline interfaces considerably alters the shearing behavior and deformation mechanisms of tilt GBs. This conclusion is of primary importance in atomistic modeling because the deformation of bicrystals and more complex GB networks have commonly been modeled with perfectly-flat GB structures in the classical Voronoï construction used for past atomistic studies, with no consideration for random GB defects. However, recent experimental observations using a new nanodiffraction technique [18, 19] have revealed that GBs in columnar-grained Cu obtained by DC magnetron sputtering have defective structures not yet accounted for in theoretical models. It is therefore imperative to understand the role of GB defects, such as nanovoids, on plastic deformation processes since the deformation of the GB network governs the overall plasticity of nanocrystalline and nanotwinned metals [45].

First, GB-mediated dislocation emission is an important mechanism in the dependence of hardness and tensile strength on grain size in nanocrystalline metals, as well as in twin-dislocation interaction mechanisms controlling the plasticity and fracture of nanotwinned metals [12, 45, 46]. The present simulations have shown that voids could constitute the preferential sites for dislocation emission. In LAB, this phenomenon only becomes noticeable when the void size exceeds 4 Å. In HAB, however, the void size must attain 8 Å. This discrepancy between LAB and HAB could be attributed to the effect of grain misorientation on local stress concentrations induced by voids at the interface [33]. Also, this result is in good agreement with the atomistic work of Wang et al. [19] in which "defective" GBs were simulated by introducing 5-Å gaps between neighboring grains and relaxing the interfaces, which led to a 50% reduction in the yield stress to emit dislocations from GBs under tensile

loading.

A second important mechanism in nanocrystalline metals is related to GB sliding by atom shuffling, which was found responsible for the so-called "inverse" Hall-Petch effect in the literature, i.e., a decrease of strength with decreasing grain size below 20-50 nm. In the present study, voids were found to reduce the amount of atom shuffling by locally shielding the applied shear stress. Also, a void size effect was found to result in a transition from GB sliding to dislocation emission for large voids of 10 Å. This finding suggests that shear stresses may be more concentrated on the voids at a critical size. At the macroscopic scale, the above predictions suggest that defective GBs could alter the critical grain size at which the inverse Hall-Petch effect starts to operate in nanocrystalline materials.

Third, shear-coupled GB migration corresponds to a deformation process for which a crystalline interface is displaced in the direction perpendicular to the GB plane when subjected to pure shear loading along its tangential direction [6]. In particular, a discontinuous grain growth in nanocrystalline metals has been largely attributed to this phenomenon in the recent literature [7]. However, the factors influencing grain growth and shear-coupled GB migration in nanocrystalline metals remain an open question. For example, GB migration does not always occur at low temperature or when some impurities have diffused along the GBs [47]. In the present study, although temperature and impurities have not been considered, we find that voids can stop either fully or partially the GB migration which, to our knowledge, has never been reported so far. We have also predicted that GB migration modes depend on the size of voids. Another interesting finding is that dislocation emission from nanovoids can be predominant over plastic deformation for certain GB types, such as $\Sigma27(115)$ GBs. We therefore conclude that it is important to consider intrinsic GB defects when both mechanisms occur concurrently.

## 4.2. Void-induced local stress

The differences in deformation mechanism between the GB interfaces when voids are present suggest that local stresses induced by the voids play an important role. To test this idea, we theoretically treat the behavior of defective GBs using a composite model for which perfect GB segments without voids offer a positive resistance $\sigma_{max_0}$ as predicted in Figure 2, while nanovoids are associated with a residual stress $\sigma_v$ acting in the vicinity of the defect. The limit of elasticity of a defective GB interface can be expressed by

$$\sigma_{max} = (1 - V) * \sigma_{max_0} + V * \sigma_v \tag{1}$$

where $V$ is the volume fraction of voids with respect to the GB volume. For the later, a GB thickness ranging from 0.5 to 1 nm, or about 2 to 5 atomic layers, has frequently been chosen in previous studies [48, 49]. The void volume fraction $V$ corresponds to the ratio of the amount of removed atoms from the GB and the average number of atoms taken for an assumed 1 $nm$ GB thickness ($\approx$1500 atoms). For example, for the $\Sigma 5(210)$ GB, in the case of 16 voids of size 10 Å, 142 atoms have been removed, leading to a maximum void volume fraction over all simulations equal to $142/1500 = 9.47\%$. Also, 4 voids of size 10 Å for the HAB leads to a maximum value of $V$ over the 4 voids simulations of about 2.51%, which is close to the fractions reported in bulk studies [24] ranging from 1% to 5%. For brevity, only the 4 Å and 8 Å cases have been detailed here ; however, we assert that the same trends have been observed for larger void volume fractions. Determining the GBs' thickness this way may look coarse and somehow simple in view of the tools we have to describe exactly the thickness of each GB, for example, by either finding the atoms with energy above the bulk energy in the unstressed bi-crystals or using the centrosymmetry analysis. The problem with these numerical approaches is that the void volume fractions would be hardly comparable from one GB to the other because of the large variability in GBs' thicknesses ; for example,

11

the number of atoms constituting a HAB being more important than in a LAB. Also, based on our observations, GBs are not relaxed uniformly along the interface, and crystal defects can stand quite far from this interface. In view of the multifactorial nature of the problem and of the desire to standardize the conditions of the simulations and the determination of $V$, we have chosen a value admittedly arbitrary, but having the advantage of being both simple and fair to all GBs considered. Re-writing Equation (1) gives

$$\frac{\sigma_{max}}{\sigma_{max_0}} = 1 - V * (1 - \frac{\sigma_v}{\sigma_{max_0}}) \qquad (2)$$

Equation (2) enables us to estimate the void-induced stresses $\sigma_v$ in each GB by directly measuring the slope between the ratio $\sigma_{max}/\sigma_{max_0}$ and $V$ from data presented in Figure 3. Figure 8 shows that in the case of 4 voids inserted in different GBs the dependence of $\sigma_{max}/\sigma_{max_0}$ with $V$ not only is linear, which supports our hypothesis, but also strongly deviates from a slope of -1 corresponding to $\sigma_v = 0$. Remarkably, Figure 8 also shows that the slope changes sharply between the different GB structures studied, indicative of significant variations in the void-induced stresses. We show in Table 1 that voids are associated with strong negative shear stresses $\sigma_v$ that are competing against the (positive) applied shear stress. This conclusion is also valid when considering 8 voids in the GBs. Therefore, in the following, we only focus on the results obtained with 4 voids per GB.

First, Figure 8 shows that the HAB interface presents a lower slope (-5.96) than the LAB interface because ED and EV processes occurred simultaneously. In LAB, a higher shear stress is applied on voids and, consequently, the EV process is activated sooner than for the HAB case, thereby explaining why dislocations are more preferentially emitted from voids in the LAB than the HAB. For the GBs involved in the migration mechanism, *i.e.* $\Sigma 5(210)$ and $\Sigma 27(115)$ GBs, Figure 8 shows that a steeper slope may likely due to less perturbations in the GB migration from HT or EV. For the $\Sigma 9(221)$ GBs, which deform

12

by sliding, voids act as strong pinning points against shuffling and the slope is the steepest (-34.4). This result therefore supports the idea that the influence of nanovoids in blocking shuffling in the $\Sigma 9(221)$ GB could be attributed to strong shear stress shielding effects near the voids.

Second, we further confirm the significance of void-induced stresses by analyzing the changes in the virial stress on each atom. The computational technique used here to achieve the stresses at the atomic level is based on a previous MD study [50] where the volume of each atom was estimated from a 3D Voronoï tessellation performed at each displacement increment. In this way, the virial stress in the present study was more accurately determined for each atom and presented all real stress characteristics. Besides, the virial stress is commonly used to deduce atomistic mechanisms as, for instance, in [15, 51]. Figures 9(a) and 9(b) show that the von Mises stress at atomic level is higher in the presence of voids in the $\Sigma 5(210)$ GB. We note that the stress at the boundary reaches 4.2GPa (see Figure 9(a)) when the applied shear stress is only about 0.6 GPa (see Table 1). This stress discrepancy between the boundary and the topmost row of nodes, observed for each GB, lies in the fact that the local stress is highly non-homogeneous with positive and negative values at the GB where defects are present. The maximum stress computed is 5.466 GPa when voids are inserted and only 4.225 GPa without voids. This suggests that vacancy defects rise the magnitude of local von Mises stresses at GBs. We also note that, although the equivalent von-Mises stress is only positive, large negative shear stresses were found near the voids. Similarly, Figures 9(c) and 9(d), presenting the results for the LAB interface, show higher stresses near voids (3.615 GPa compared to 3.199 GPa without voids). Finally, Figures 9(e) and (f) for the $\Sigma 9(221)$ GB (with and without voids) show that the stresses around voids (5.388 GPa) are particularly strong compared to those in the perfect GB (3.365 GPa). The stress difference (2.022 GPa) in this type of GB is significantly larger than in the other types, i.e. 1.241 GPa and 0.416 GPa in $\Sigma 5(210)$ and LAB, respectively. This result is consistent with the larger

13

slope observed for $\Sigma9(221)$ GBs in Figure 8, and modeled by Equation (2), as a function of the void volume fraction $V$.

## 5. Conclusion

QC simulations of tilt $\Sigma$, HAB and LAB bicrystals undergoing simple shear loading have shown that vacancy defects and nanovoids introduced at the interface result in significant GB softening that leads to a linear decrease of the yield strength with respect to the void volume fraction. Nanovoids are found to play crucial roles on GB deformation in shear due to void-induced stresses. New deformation mechanisms emerged from this study, depending upon the number and size of the nanovoids involved. First, nanovoids were found to act as pinning points that impede atom shuffling across the interfaces. Second, dislocations were found to be preferentially emitted from voids, instead of intrinsic GB sites ; more so in LAB interfaces than in HAB interfaces. Third, the effect of nanovoids on shear-coupled migration was found to depend on the GB type. For the $\Sigma5(210)$ GB, migration is not significantly affected and no dislocation emission is observed. On the contrary, $\Sigma27(115)$ GB undergoes significant perturbations in its migration and preferentially emits dislocations when voids become large. On a final note, our simulations were performed at the limit for which voids are treated as non-interacting. Therefore, studying the behavior of GBs with closer voids could also help in understanding the mechanisms involved at this scale. These findings underscore the importance of nanovoids and defective GBs in understanding complex deformation processes such as shear banding in GB networks or plasticity in nanocrystalline and nanotwinned metals.

14

# References

[1] Y. S. Li, N. R. Tao, K. Lu, Acta Materialia 56 (2008) 230–41.

[2] P. E. Donovan, W. M. Stobbs, Acta Metallurgica 31 (1983) 1–8.

[3] J. Li, Z. L. Wang, T. C. Hufnagel, Physical Review B 65 (2002) 144201–1 144201–6.

[4] F. Sansoz, V. Dupont, Materials Science and Engineering C 27 (2007) 1509–13.

[5] F. Sansoz, V. Dupont, Applied Physics Letters 89 (2006).

[6] J. W. Cahn, Y. Mishin, A. Suzuki, Acta Materialia 54 (2006) 4953–75.

[7] D. S. Gianola, S. Van Petegem, M. Legros, S. Brandstetter, H. Van Swygenhoven, K. J. Hemker, Acta Materialia 54 (2006) 2253–63.

[8] M. Legros, D. S. Gianola, K. J. Hemker, Acta Materialia 56 (2008) 3380–93.

[9] T. J. Rupert, D. S. Gianola, Y. Gan, K. J. Hemker, Science 326 (2009) 1686–90.

[10] V. Dupont, F. Sansoz, Acta Materialia 56 (2008) 6013–26.

[11] H. Van Swygenhoven, M. Spaczer, A. Caro, D. Farkas, Physical Review B 60 (1999) 22–5.

[12] K. S. Kumar, H. Van Swygenhoven, S. Suresh, Acta Materialia 51 (2003) 387–405.

[13] J. Schiøtz, K. W. Jacobsen, Science 301 (2003).

[14] F. Sansoz, K. D. Stevenson, Physical Review B 83 (2011) 224101–1 224101–9.

[15] J. Schiøtz, F. D. Di Tolla, K. W. Jacobsen, Nature 391 (1998).

[16] H. Van Swygenhoven, P. M. Derlet, Physical Review B 64 (2001).

[17] F. Sansoz, V. Dupont, Scripta Materialia 63 (2010) 1136–9.

[18] T. LaGrange, B. W. Reed, M. Wall, J. Mason, T. Barbee, Applied Physics Letters 102 (2013) 011905–1 011905–5.

[19] Y. M. Wang, F. Sansoz, T. LaGrange, R. T. Ott, J. Marian, T. W. Barbee Jr., H. A. V., Nature Materials 12 (2013) 697–702.

[20] A. G. Frøseth, H. Van Swygenhoven, P. M. Derlet, Acta Materialia 53 (2005) 4847–56.

[21] A. Strachan, T. Cagin, W. Goddard, Physical Review B 63 (2001).

[22] R. Rudd, J. Belak, Computational Materials Science 24 (2002) 148–53.

[23] H. A. Wu, G. R. Liu, J. S. Wang, Modelling and Simulation in Materials Science and Engineering 12 (2004) 225–33.

[24] X. Yang, T. Zhou, C. Chen, Computational Materials Science 40 (2006) 51–6.

[25] M. Changwen, D. A. Buttry, P. Sharma, D. A. Kouris, Journal of Mechanics and Physics of Solids 59 (2011) 1858–71.

[26] T. Frolov, D. L. Olmsted, M. Asta, Y. Mishin, Nature Communications (2013).

[27] V. B. Shenoy, R. Miller, E. B. Tadmor, D. Rodney, R. Phillips, M. Ortiz, Journal of Mechanics and Physics of Solids 47 (1999) 611–42.

[28] R. Miller, E. B. Tadmor, Journal of Computer-Aided Materials Design 9 (2002) 203–39.

[29] F. Sansoz, J. F. Molinari, Scripta Materialia 50 (2004) 1283–8.

[30] F. Sansoz, J. F. Molinari, Acta Materialia 53 (2005) 1931–44.

[31] V. Péron-Lührs, A. Jérusalem, F. Sansoz, L. Stainier, L. Noels, Journal of Mechanics and Physics of Solids 61 (2013) 1895–914.

[32] J. Marian, J. Knap, M. Ortiz, Acta Materialia 53 (2005) 2893–900.

[33] I. Milas, Y. Qi, B. W. Sheldon, V. B. Shenoy, Journal of Applied Physics 109 (2011) 033518–1 033518–8.

[34] D. E. Spearot, M. A. Tschopp, K. I. Jacob, D. L. McDowell, Acta Materialia 55 (2007) 705–14.

[35] D. B. Shan, L. M. Wang, L. Yuan, Journal of Materials Research 28 (2013) 766–73.

[36] Y. F. Shao, X. Yang, X. Zhao, S. Q. Wang, Chinese Physics B 21 (2012).

[37] A. King, G. Johnson, D. Engelberg, W. Ludwig, J. Marrow, Science 321 (2008) 382–5.

[38] M. A. Arafin, J. A. Szpunar, Corrosion Science 51 (2009) 119–28.

[39] L. N. Brewer, M. A. Othon, L. M. Young, T. M. Angeliu, Microscopy and Microanalysis 12 (2006) 85–91.

[40] N. Shigematsu, D. J. Prior, J. Wheeler, Journal of Microscopy 224 (2006) 306–21.

[41] S. M. Foiles, M. I. Baskes, M. S. Daw, Physical Review B 33 (1986) 7983–91.

[42] M. S. Daw, S. M. Foiles, M. I. Baskes, Materials Science Reports 9 (1992) 251–310.

[43] M. F. Horstemeyer, M. I. Baskes, V. C. Prantil, J. Philliber, S. Vonderheide, Modelling and Simulation in Materials Science and Engineering 11 (2003).

[44] C. L. Kelchner, S. J. Plimpton, J. C. Hamilton, Physical Review B 60 (1998) 11085–8.

[45] Z. You, X. Li, L. Gui, Q. Lu, H. Zhu, T. Gao, L. Lu, Acta Materialia 61 (2013) 217–27.

[46] C. X. Huang, K. Wang, S. D. Wu, Z. F. Zhang, G. Y. Li, S. X. Li, Acta Materialia 54 (2006) 655–65.

[47] J. C. M. Li, Physical Review Letters 96 (2006).

[48] G. J. Thomas, R. W. Siegel, J. A. Eastman, Scripta Metallurgica and Materialia 24 (1990) 201–9.

[49] H. Kung, P. G. Sanders, J. R. Weertman, Advanced Materials for the twenty-first Century (1999) 455–63.

[50] G. Szefer, D. Jasińska, Bulletin of the Polish academy of sciences, technical sciences 57 (2009).

[51] F. Cleri, S. Yip, D. Wolf, S. R. Phillpot, Physical Review Letters 79 (1997).

## Figure captions

FIGURE 1: Quasicontinuum modeling of a tilt bicrystals containing nanovoid defects at the interface. a) Schematics of atomistic and continuum zones, and crystal orientations for a $\Sigma9(221)$ GB. b) Boundary conditions for zero force lattice relaxation used to simulate 0 K equilibrium GB structures. Voids are represented with dashed lines. c) Atomistic snapshot before relaxation for a $\Sigma9(221)$ GB in Cu with a void volume fraction equal to 1.48% (4 voids, diameter 10 Å). Bright-colored atoms are in perfect fcc crystal lattice (zero centrosymmetry). Dark-colored atoms are part of crystal defects (non-zero centrosymmetry).
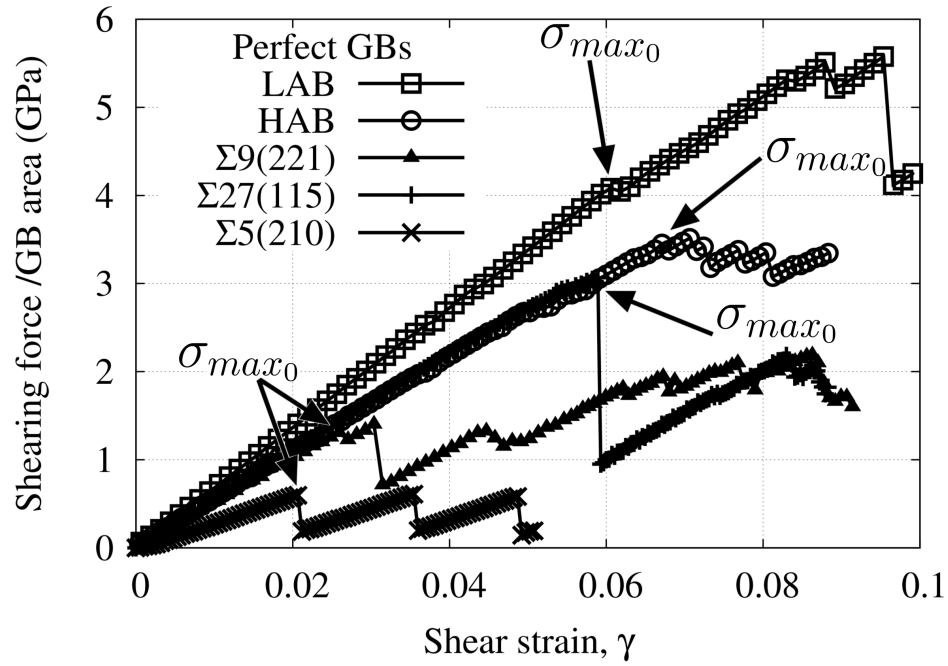
FIGURE 2: Shear stress *vs.* $\gamma$ curves for different GBs (LAB, HAB, $\Sigma9(221)$, $\Sigma27(115)$, $\Sigma5(210)$) in Cu in the absence of voids. $\sigma_{max_0}$ is the maximum stress reached by all GBs without voids at the plastic deformation onset.
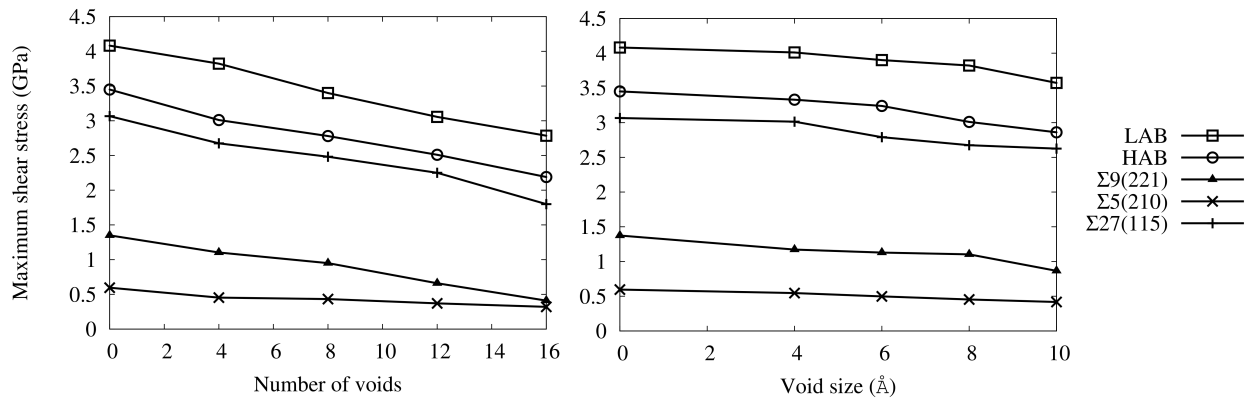
FIGURE 3: Dependence of the maximum shear stress with respect to a) the number of voids (size 8 Å), and b) the void size (4 voids).
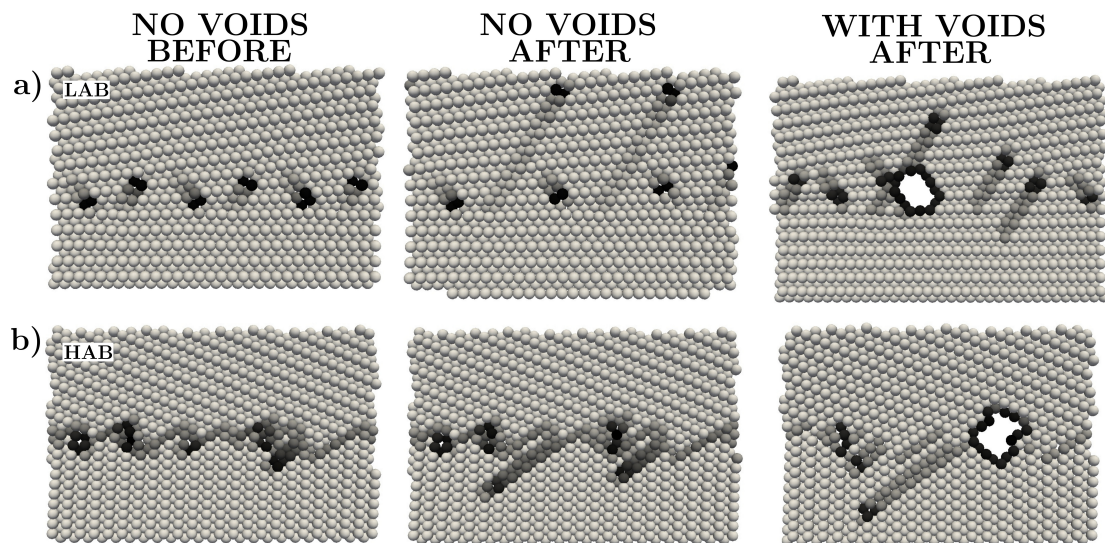
FIGURE 4: GB-mediated dislocation emission in LAB and HAB interfaces (partial views of the GBs). Dislocations are emitted by either mismatch interface defects (ED) or voids (EV) at the yield point. a) LAB before and after yielding mediated by ED (0 voids), and after with a void size of 10 Å mediated by EV. b) HAB before and after yielding mediated by EV without voids, and after yielding with a void size 10 of Å.
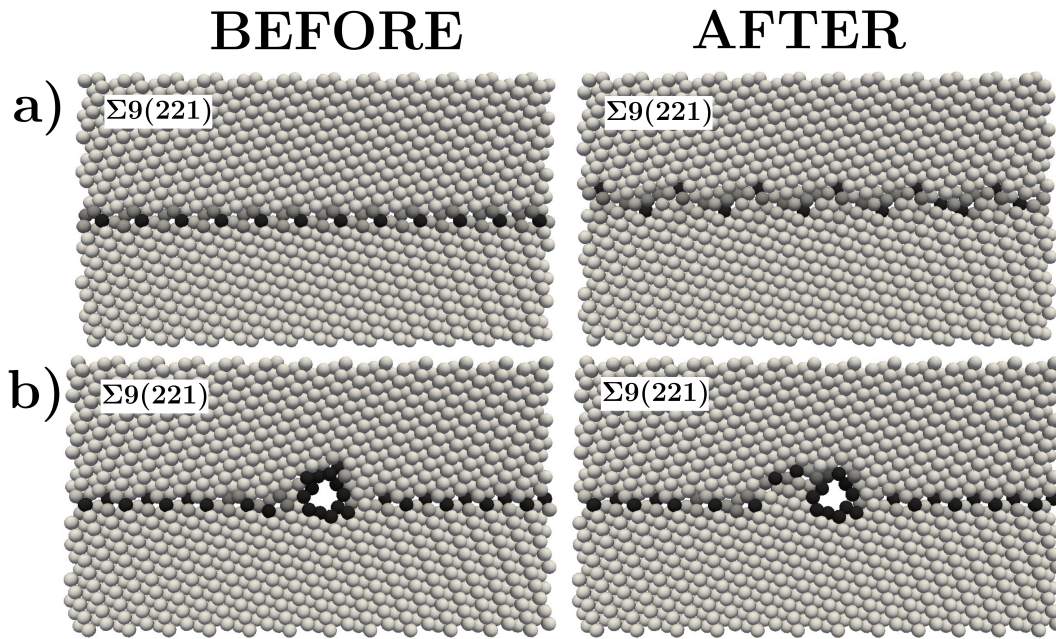
FIGURE 5: Σ9(221) GB sliding by atom shuffling deformation mode (partial views of the GBs). a) Homogeneous shuffling (HS) before and after yield point. b) Partial shuffling from voids (PS) before and after yield point.
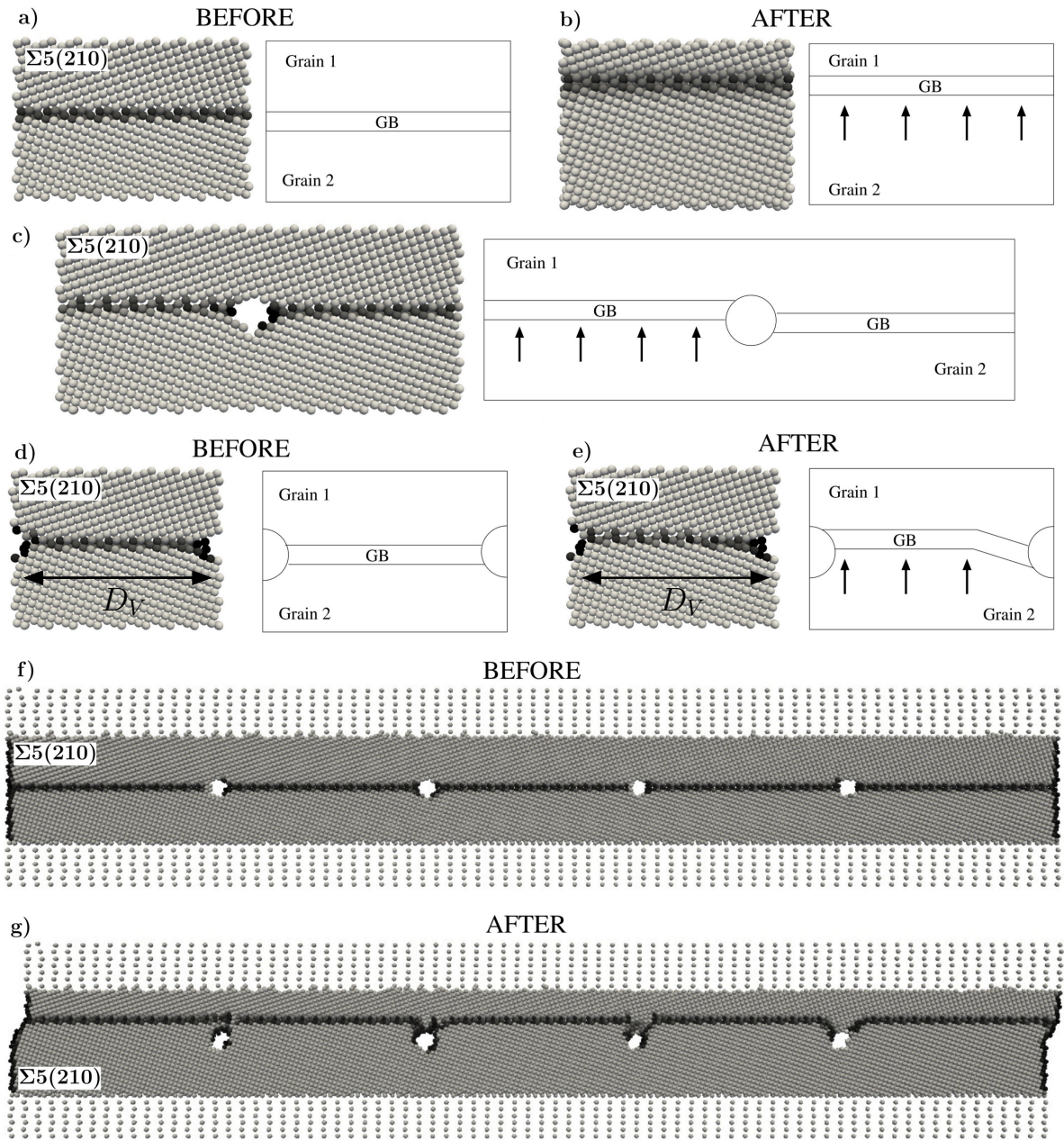
FIGURE 6: Shear-coupled GB migration processes in $\Sigma5(210)$ GB. a), b) Homogeneous and total GB migration (HT) before and after plastic deformation. c) Homogeneous and partial GB migration (HP) after yield point (4 voids, size 8 Å). d), e) Inhomogeneous and partial GB migration (IP) before and after yield point (8 voids, size 8 Å). Only partial views of the GBs are shown in a)-e). Full view of the GB (4 voids, size 10 Å) f) just after the relaxation step and g) reformation of the migration front.
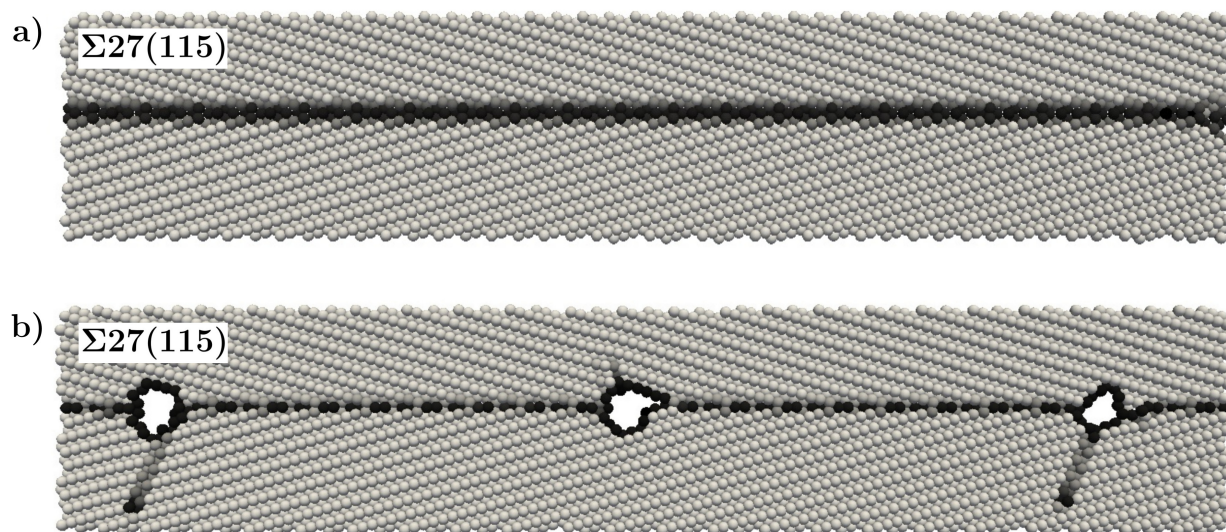
FIGURE 7: Deformation processes in $\Sigma 27(115)$ GBs (only partial views of GBs). a) Shear-coupled migration of GB without voids after first migration step. b) Defective GB (4 voids of size 10 Å) for which incipient plasticity is activated from voids by partial dislocations emissions.
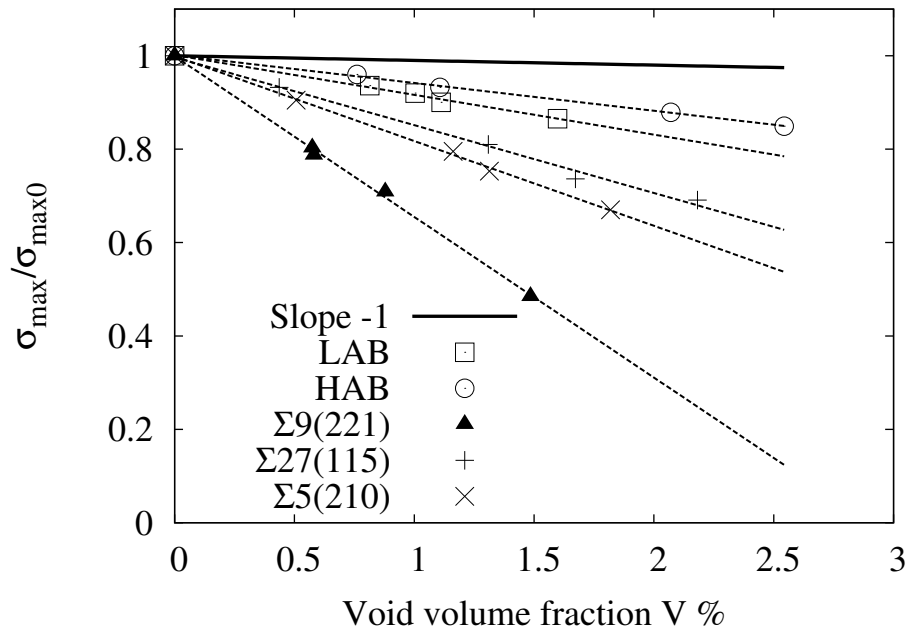
FIGURE 8: Fitting of $\sigma_{max}/\sigma_{max_0}$ *vs.* void volume fraction $V$ by Equation (2) (dashed lines) for models containing 4 voids. The model predictions with no void-induced stress ($\sigma_v = 0$) are shown with a solid line for comparison.
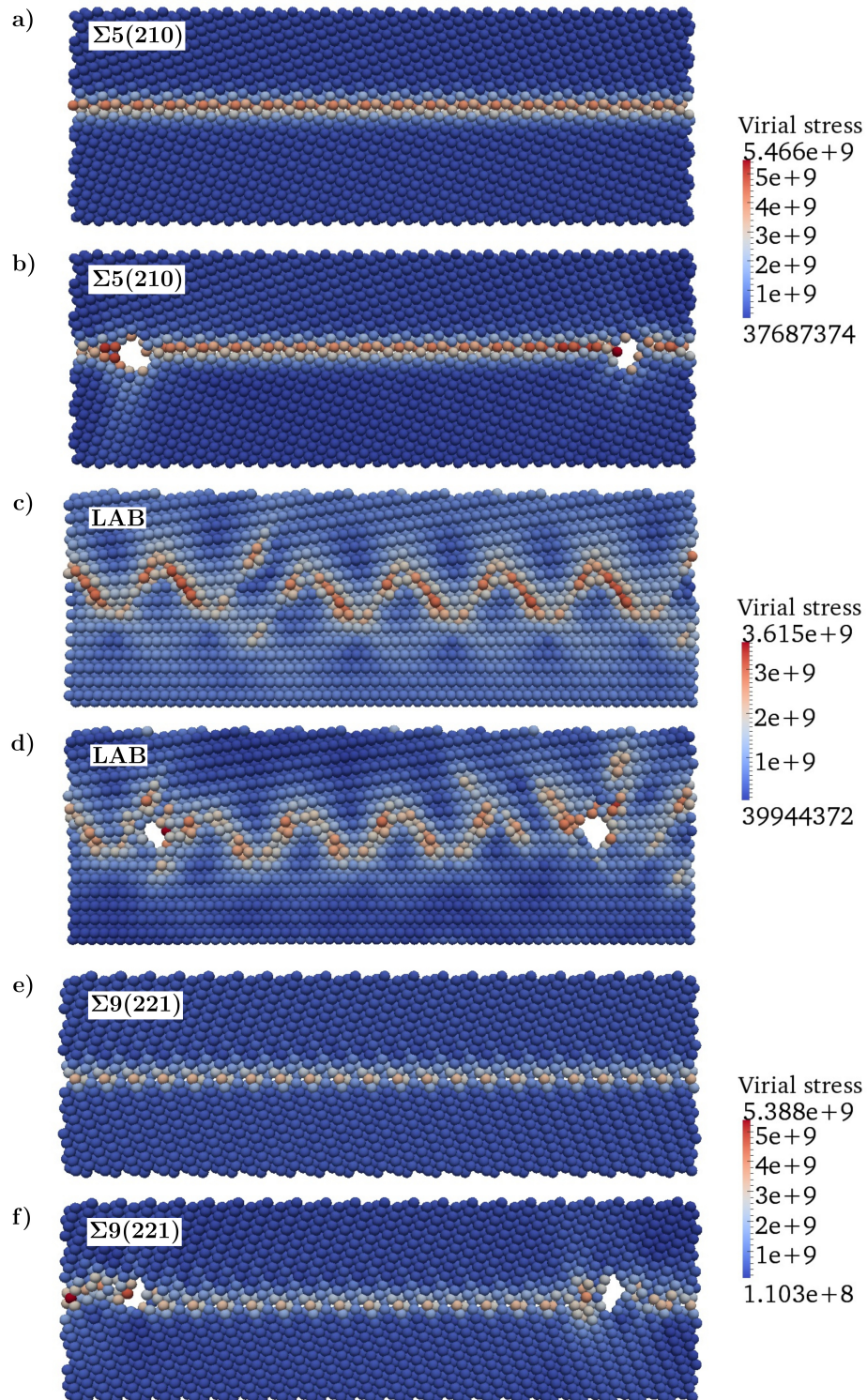
FIGURE 9: Virial stress (von Mises) (Pa) snapshots (partial views of the GBs) before yield point when a) no void and b) voids are inserted in a $\Sigma 5(210)$ GB (4 voids, size 8 Å). c) and d) same analysis for a LAB interface. e) and f) ditto for a $\Sigma 9(221)$ GB.

**Table captions**

TABLE 1: Maximum shear strength of perfect GBs, $\sigma_{max_0}$, and void-induced stresses $\sigma_v$ for each GB in which 4 or 8 voids –successively of different sizes– are inserted.

| GB type | Number of voids | | | | |
| | 0 | 4 | | 8 | |
| | $\sigma_{max_0}$ (GPa) | Slope in Eq. (2) | $\sigma_v$ (GPa) | Slope in Eq. (2) | $\sigma_v$ (GPa) |
|---|---|---|---|---|---|
| LAB | 4.08 | -8.51 | -30.6 | -7.71 | -27.4 |
| HAB | 3.45 | -5.96 | -17.1 | -5.87 | -16.8 |
| $\Sigma 9(221)$ | 1.35 | -34.4 | -45.1 | -39.3 | -51.7 |
| $\Sigma 27(115)$ | 3.07 | -14.5 | -41.4 | -13.4 | -38.1 |
| $\Sigma 5(210)$ | 0.60 | -18.1 | -10.3 | -19.4 | -11.0 |

Table 2: Deformation modes in defective GBs as a function of the number of voids and void size. HT : homogeneous and total GB migration. HP : homogeneous and partial GB migration. IP : inhomogeneous and partial migration. EV : dislocation emission from voids. ED : dislocation emission periodic defects. HS : homogeneous shuffling. PS : partial shuffling.

| Deformation of perfect GB | GB type | Number of voids | Void sizes (Å) | | | |
|---|---|---|---|---|---|---|
| | | | 4 | 6 | 8 | 10 |
| Dislocation emission from periodic defects ED | LAB | 4 | ED | ED | EV | EV |
| | | 8 | ED | ED | EV | EV |
| Dislocation emission from periodic defects ED | HAB | 4 | ED | ED+EV | ED+EV | EV |
| | | 8 | ED | ED+EV | ED+EV | EV |
| Atom shuffling HS | Σ9(221) | 4 | HS | PS | PS | PS |
| | | 8 | HS | PS | PS | EV |
| GB migration HT | Σ27(115) | 4 | HT+EV | HP+EV | EV | EV |
| | | 8 | HT+EV | IP+EV | EV | EV |
| GB migration HT | Σ5(210) | 4 | HT | HT | HP | HP |
| | | 8 | HT | HT | IP | IP |